Computers, Materials & Continua CMC, vol.64, no.1, pp.313-323, 2020

Efficient Strip-Mode SAR Raw-Data Simulator of Extended Scenes Included Moving Targets Based on Reversion of Series

Liang Yang[1, *], Daojian Zeng[2], Jianhua Yan[3] and Yaozhang Sai[1]

Abstract: The Synthetic Aperture Radar (SAR) raw data generator is required to the evaluation of focusing algorithms, moving target analysis, and hardware design. The time-domain SAR simulator can generate the accurate raw data but it needs much time. The frequency-domain simulator not only increases the efficiency but also considers the trajectory deviations of the radar. In addition, the raw signal of the extended scene included static and moving targets can be generated by some frequency-domain simulators. However, the existing simulators concentrate on the raw signal simulation of the static extended scene and moving targets at uniform speed mostly. As for the issue, the two-dimensional signal spectrum of moving targets with constant acceleration can be derived accurately based on the geometric model of a side-looking SAR and reversion of series. And a frequency-domain algorithm for SAR echo signal simulation is presented based on the two-dimensional signal spectrum. The raw data generated with proposed method is verified by several simulation experiments. In addition to reveal the efficiency of the presented frequency-domain SAR scene simulator, the computational complexity of the proposed method is compared with the time-domain approach using the complex multiplication. Numerical results demonstrate that the present method can reduce the computational time significantly without accuracy loss while simulating SAR raw data.

Keywords: Raw data simulation, moving target, reversion of series.

1 Introduction

Computer simulation plays an important role in every field [Zhang, Duan, Liu et al. (2019); Wang, Zeng, Patterson et al. (2019)]. Synthetic Aperture Radar (SAR) is a well-established remote sensing instrument in all weather conditions and day and night [Xiong, Jin, Xu et al. (2019)]. As the most important applications for SAR, the performance of the ground moving targets indication (GMTI) system can be analyzed and evaluated by modeling the whole system using simulation method [Sjogren, Vu, Peterson et al. (2012); Lv, Wang and Liu (2013); Li, Liu, Wang et al. (2019)]. The SAR raw data generator is required to the evaluation of focusing algorithms, moving target analysis, and hardware design [Franceschetti, Migliaccio, Riccio et al. (1992); Wang, Zhang and Deng

[1] School of Information and Electrical Engineering, Ludong University, Yantai, 264025, China.

[2] Changsha University of Science & Technology, Changsha, 410004, China.

[3] Mathematics Department, Florida Atlantic University, Florida, 33431, USA.

[*] Corresponding Author: Liang Yang. Email: yangliang_mail@163.com.

Received: 20 January 2020; Accepted: 08 March 2020.

(2008); Franceschetti, Guida, Iodice et al. (2004); Qiu, Hu, Zhou et al. (2010)]. The time-domain method can achieve a realistic simulation but it is highly time consuming especially in the present of extended scenes [Mori and Vita (2004)]. The frequency-domain approach can highly reduce the computational load, which can accommodate the space-varied range-azimuth coupling and the senor trajectory deviations exactly [Franceschetti, Iodice, Perna et al. (2006); Chen, Guo, Wu et al. (2019); Jin, Liu, Deng et al. (2019)].

Some SAR raw data generators can simulate the raw data of moving targets. Dogan proposed an efficient SAR raw data simulator which can generate the raw signal of moving targets with constant speed [Dogan and Kartal (2011)]. However, the precision of the simulator is not high enough because of using the hyperbolic approximation during the derivation of the spectrum of the moving targets. Thus, yang presented an efficient generator based on the derived accurate spectrum of the moving target [Yang, Yu, Gao et al. (2013); Yang, Yu, Luo et al. (2013)]. The existing simulators concentrate on the raw signal simulation of moving targets at uniform speed mostly. As for the issue, the two-dimensional signal spectrum of moving targets with constant acceleration can be derived accurately based on the reversion of series method in the paper. And a frequency-domain algorithm for SAR echo signal simulation is presented based on the two-dimensional signal spectrum. The simulation results validate the effectiveness of the proposed simulator.

The letter is organized as follows. Section 2 presents the theory of the proposed raw signal simulation approach using the method of reversion of series. Section 3 introduces the procedure of the proposed simulator. In Section 4, the simulator is validated by point target simulations. The efficiency is analyzed in Section 5. Conclusions are reported in Section 6.

2 Geometry configuration and two-dimensional signal spectrum

The SAR geometric configuration is shown as Fig. 1. In this figure, O stands for the start point, t represents the slow time, v is the SAR platform velocity. A moving target denoted by $P(R_0, x_0)$ is located in the static scene with velocity and constant acceleration (v_r, a_r) in the slant range direction and (v_a, a_a) in the azimuth direction. And the platform height is H, the closest slant range from the platform to the point target $P(R_0, x_0)$ is R_0.

According to the geometry in Fig. 1, the slant range between the platform and the target can be expressed as

$$R(t) = \sqrt{\left[x_0 + v_r t + \frac{1}{2} a_r t^2\right]^2 + \left[(v - v_a)t + \frac{1}{2} a_a t^2\right]^2 + H^2} \tag{1}$$

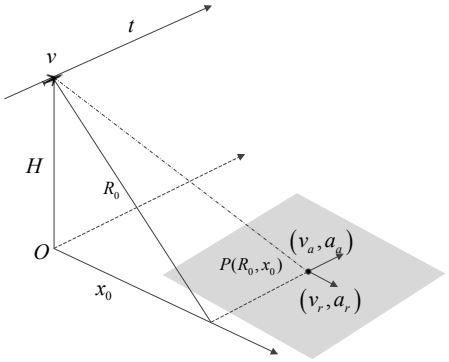

Figure 1: Strip-mode geometry

It is difficult to obtain analytical spectrum of system transfer function using the principle of stationary phase (POSP). In the paper we derive the analytical spectrum of the moving target with constant acceleration using the series inversion method. Applying Taylor expansion for Eq. (1), the expression is shown as

$$R(t) = R_0 + k_1 t + k_2 t^2 + k_3 t^3 \tag{2}$$

where

$$R_0 = \sqrt{x_0^2 + H^2}\ ,\ k_1 = \frac{x_0 v_r}{\sqrt{x_0^2 + H^2}} = \frac{M}{R_0}\ ,\ k_2 = \frac{1}{2}\left[\frac{v_r^2 + \left(v - v_a\right)^2 + x_0 a_r}{x_0^2 + H^2} - \frac{x_0 v_r}{\left(x_0^2 + H^2\right)^{3/2}}\right] = \frac{2N}{R_0} - \frac{2M^2}{R_0^{\ 3}}\ ,$$

$$k_3 = \frac{3P}{R_0} - \frac{3MN}{R_0^{\ 3}} + \frac{3M^3}{R_0^{\ 5}}\ .$$

where M, N, P is expressed as

$$M = x_0 v_r, N = v_r^2 + \left(v - v_a\right)^2 + x_0 a_r, P = \left(v - v_a\right) a_a + v_r a_r\ .$$

The more the expansion order is, the more accurate the imaging error is. However, as the expansion order increases, the computational complexity increases dramatically. While the phase error introduced is less than $\pi/4$, the influence can be ignored for SAR image. Expanding $R(t)$ to third-order, we can find that the expansion error satisfies the condition. Thus, the accurate echo can be obtained by expanding the distance to third-order in this paper.

Suppose the received baseband signal from a point target is

$$S\left(\tau, t\right) = \sigma\left(R_0, x_0\right) \cdot w_r\left(\tau - \frac{2R\left(t\right)}{c}\right) w_a\left(t\right) \cdot \exp\left[-j4\pi f_0 R\left(t\right)/c\right] \cdot \exp\left[j\pi K_r \left(\tau - 2R\left(t\right)/c\right)^2\right] \tag{3}$$

where $\sigma\left(R_0, x_0\right)$ is the reflectivity coefficient of the point target, $w_r(\cdot)$ and $w_a(\cdot)$ is the range and azimuth window function of radar echo signal respectively, τ and t represents the range and azimuth time variables respectively, c is the speed of light, f_0 is the carrier frequency, K_r is the chirp rate.

Using the series inversion method and performing two-dimensional Fourier transformation (FT), we obtain

$$H\left(f_\tau, f_t\right) = w_r\left(f_\tau\right) w_a\left(f_t\right) \exp\left[j\Psi\left(f_\tau, f_t\right)\right] \tag{4}$$

where f_τ, f_t denotes the range and azimuth frequency respectively.

$$\Psi\left(f_\tau, f_t\right) = \Psi_0\left(f_t\right) + \Psi_1\left(f_t\right) f_\tau + \Psi_2\left(f_t\right) f_\tau^2 \tag{5}$$

where

$$\Psi_0\left(f_t\right) = -2\pi f_0 \frac{2R_0}{c} + \frac{\pi c f_t^2}{4 f_0 k_2} + \frac{\pi k_1 f_t}{k_2} + \frac{\pi f_0 k_1^2}{c k_2} + \frac{\pi c^2 k_3 f_t^3}{16 f_0^2 k_2^3} + \frac{3\pi c k_1 k_3 f_t^2}{8 f_0 k_2^3} + \frac{3\pi k_1^2 k_3 f_t}{4 k_2^3} + \frac{\pi f_0 k_1^2 k_3}{2 c k_2^3}$$

$$\Psi_1\left(f_t\right) = -\frac{4\pi R_{ref}}{c} - \frac{\pi c f_t^2}{4 k_2 f_0^2} + \frac{\pi k_1^2}{c k_2} - \frac{\pi c^2 k_3 f_t^3}{8 f_0^3 k_2^3} - \frac{3\pi c k_1 k_3 f_t^3}{8 f_0^2 k_2^3} + \frac{\pi k_1^3 k_3}{2 c k_2^3}$$

$$\Psi_2\left(f_t\right) = -\frac{\pi}{K_r} + \frac{\pi c f_t^2}{4 k_2 f_0^3} + \frac{3\pi c^2 k_3 f_t^3}{16 k_2^3 f_0^4} + \frac{3\pi c^2 k_1 k_3 f_t^3}{8 f_0^3 k_2^3}$$

.

$\Psi_0(\cdot)$ is unrelated to the range frequency f_τ, which stands for the azimuth modulation. $\Psi_1(\cdot)$ is the linear term coefficient of the range frequency f_τ, which represents the range migration of the moving target. $\Psi_2(\cdot)$ is the square term coefficient of f_τ.

The obtained SAR two-dimensional spectrum of moving target with constant acceleration is the first key step to develop a frequency-domain raw signal simulation approach. We will introduce the raw data simulation procedure in detail in the next section.

3 Raw data simulation

The SAR raw data simulation procedure for the extended scene included fixed point target (FPT), fixed distributed target (FDT), moving point target (MPT) and moving distributed target (MDT), we can adopt the method in Yang et al. [Yang, Yu, Gao et al. (2013)]. And the basic steps of the simulator are shown in Fig. 2.

Based on the signal spectrum model, the basic steps of the raw signal simulation are outlined as follows. The reflectivity $\sigma(R_0, x_0)$ is projected to the imaging plane, the signal can be expressed as

$$S_1(\tau, t) = \iint \sigma(R_0, x_0)\delta(\tau - \tau_0)\delta(t - t_0) d\tau_0 dt_0 \tag{6}$$

where $W_r(\tau)$, $W_a(t)$ is the antenna beam pattern in the range and azimuth directions respectively, R_{ref} is the reference slant range, τ_0 represents the propagation delay of the interested target corresponding to the one in the scene center, i.e.,

$$\tau_0 = \frac{2(R_0 - R_{ref})}{c} \tag{7}$$

Performing the Fast Fourier Transform (FFT) in the azimuth direction to transform the signal into the azimuth frequency domain and introducing a linear frequency modulated signal $H_1\left(f_t, R_0\right)$, which can simulate the space-variant.

$$H_1\left(f_t, R_0\right) = \exp\left[j 2\pi f_0 f_t 2\left(R_0 - R_{ref}\right)/c\right] \tag{8}$$

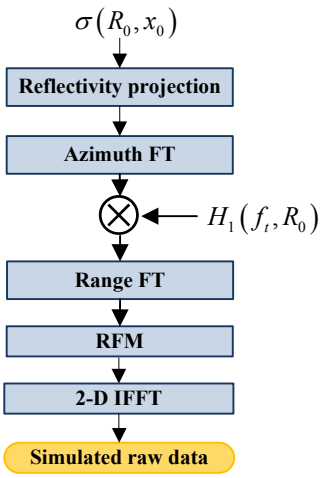

Figure 2: SAR raw signal simulator

Thus, the signal is given as

$$S_2(\tau, f_t) = \iint \sigma(R_0, t_0)\delta(\tau - \tau_0)\exp\left[j2\pi f_0 \frac{2(R_0 - R_{ref})}{c} f_t\right] \cdot \exp(-j2\pi f_t t_0) d\tau_0 dt_0 \quad (9)$$

Performing the FFT in the range direction to transform the signal into the two-dimensional frequency domain, the signal can be expressed as

$$S_3(f_\tau, f_t) = \iint \sigma(R_0, t_0)\exp\left[j2\pi f_0 \frac{2(R_0 - R_{ref})}{c} f_t\right] \cdot \exp(-j2\pi f_t t_0)\exp(-j2\pi f_\tau \tau_0) d\tau_0 dt_0 \quad (10)$$

Reference Function Multiplication (RFM) operation is applied to simulate all the range-invariant phase, thus the function is expressed as

$$H_{RFM}(f_\tau, f_t, R_{ref}) = w_r(f_\tau) w_a(f_t) \exp\left[j\Psi'(f_\tau, f_t)\right] \quad (11)$$

where

$$\Psi'(f_\tau, f_t) = \Psi_0'(f_t, R_{ref}) + \Psi_1(f_t) f_\tau + \Psi_2(f_t) f_\tau^2$$

$$\Psi_0'(f_t) = -2\pi f_0 \frac{2R_{ref}}{c} + \frac{\pi c f_t^2}{4 f_0 k_2} + \frac{\pi k_1 f_t}{k_2} + \frac{\pi f_0 k_1^2}{c k_2} + \frac{\pi c^2 k_3 f_t^3}{16 f_0^2 k_2^3} + \frac{3\pi c k_1 k_3 f_t^2}{8 f_0 k_2^3} + \frac{3\pi k_1^2 k_3 f_t}{4 k_2^3} + \frac{\pi f_0 k_1^2 k_3}{2 c k_2^3}$$

Finally, after all the above operation the raw signal is generated by applying two-dimensional Inverse Fast Fourier Transform (IFFT).

$$S_4(\tau, t) = \sigma(R_0, x_0) \cdot w_r\left(\tau - \frac{2R(t)}{c}\right) w_a(t) \cdot \exp\left[-j4\pi f_0 R(t)/c\right] \cdot \exp\left[j\pi K_r (\tau - 2R(t)/c)^2\right] \quad (12)$$

4 Simulation experiment and validation

In this section, the raw data of moving targets generated with proposed method is verified

by point targets. The velocity in the range direction will lead to the displacement of the point target in the azimuth direction, while the velocity in the azimuth direction and the acceleration in the range direction will lead to the defocusing of the target. Thus, the experiment will validate the simulated raw data of the moving targets based on the characteristic of the moving target imaging. We will measure the azimuth smear and azimuth offset after imaging of moving point targets to verify the effectiveness of the simulator. The point target simulation test will compare the two sets of values under the same parameter. The first group is the azimuth offset and smear of the target measured by the echo simulation imaging process using the simulator proposed in this paper (labeled as FD), the second group is the azimuth offset and smear measurement of the target after echo simulation imaging is performed by the time-domain method (labeled as TD). And the time-domain approach simulated the raw signal by point to point as shown in Eq. (1), which is the most accurate SAR echo simulation algorithm. Nine moving point targets with different velocities but the same range are evaluated, and last two of them are configured in squint mode. Target 1 (T1), Target 2 (T2), Target 8 (T8) and Target 9 (T9) only have range velocity, Target 3 (T3) is static target, Target 6 (T6) and Target 7 (T7) only have azimuth velocity, while Target 4 (T4) and Target 5 (T5) have two-dimensional velocity. The simulation system parameters are shown as Tab. 1. Tab. 2 gives the azimuth shifts and azimuth smear results of moving targets with different velocities but the same range.

Table 1: System parameters

Parameters	Values
Carrier Frequency	9.6 GHz
Reference Range	10 Km
Transmitted Bandwidth	150 MHz
Platform Velocity	150 m/s
Pulse Repeat Frequency	400 Hz
Pulse Length	2.5 μs
Antenna Azimuth Dimension	2 m
Squint Angle	0°/30°

Firstly, the azimuth displacement caused by the range velocity is verified and analyzed. Then 32 times interpolation analysis of the imaged target is carried out in the simulation to obtain more accurate target position information. From Tab. 2, we can see the azimuth shift induced by the range speed of moving target shows very high accuracy between time-domain method and frequency-domain method in broadside mode (T1, T2), even in the present of azimuth smear (T4, T5). In order to validate the raw signal sufficiently, we also simulate raw data of moving point target only with range velocities in squint mode (T7, T8) and the result also shows the error between frequency-domain and time-domain method is very tiny. Secondly, the azimuth defocusing caused by the azimuth direction velocity is verified and analyzed. For the moving targets with azimuth speed, we compare the point target' smear widths of 3-dB main lode between the time-domain method and the frequency-domain method to validate the accuracy of the simulated raw data. As

shown in the Tab. 2, the moving target with azimuth velocity leads to the broadening of the impact response width after imaging. With the increase of the azimuth velocity, the broadening of the impact response width deteriorates sharply (T6, T7). The azimuth smear widths based on our two-dimensional frequency-domain method is very close to the time-domain method (T6, T7), even in the present of azimuth shift (T4, T5).

Table 2: Validation

	Target velocities (v_r, v_a) m/s^2	**FD values**		**TD Values**	
		Azimuth Shift(m)	**Azimuth Smear(m)**	**Azimuth Shift (m)**	**Azimuth Smear (m)**
Broad side	T1 (1, 0)	66.6320	0.9965	66.6700	0.9973
	T2(0.5, 0)	33.3300	0.9965	33.3400	0.9973
	T3 (0, 0)	0	0.9985	0	0.9999
	T4(0.5, 1)	33.6500	1.0421	33.3300	1.0297
	T5 (1, 1)	67.5650	1.0421	66.6650	1.0297
	T6 (0, 2)	0	1.2620	0	1.2402
	T7 (0, 5)	0	6.4377	0	6.1194
Squint mode	T8 (1, 0)	66.8250	0.9955	66.6700	0.9973
	T9 (0.5, 0)	33.4200	0.9955	33.3400	0.9973

Finally, the azimuth defocusing caused by the range acceleration is verified and analyzed. The Fig. 3 shows that the impulse response width (IRW) changes with the range acceleration of the moving target after imaging process. It can be seen that with the increase of target range acceleration, IRW deteriorates sharply. Even a smaller acceleration ($0.2m/s^2$) will lead to the widening of IRW. The simulation results of (a)-(b) show that the defocusing target is well focused after the defocusing phase compensation given by Eq. (5) at different range acceleration. The accuracy of the proposed method is verified by comparing the performance of point target after phase compensation with time-domain method as shown in Tab. 3. From it we can see that the measured IRW in the azimuth direction are very close to the values of time-domain simulator. The maximum deviation of peak side lobe ratio (PSLR) in the azimuth direction is less than 0.03 dB with respect to the values of the time-domain simulator. And the measured integral side lobe ratio (ISLR) in the azimuth direction deviates from the time-domain simulator values by no more than 0.04 dB.

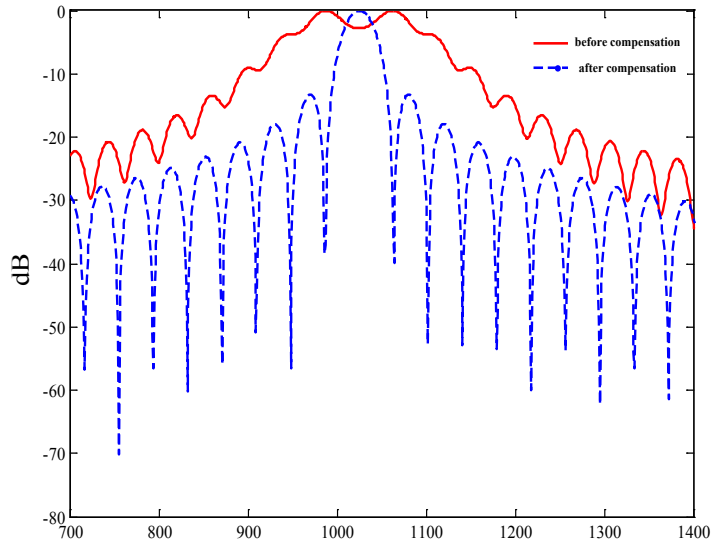

(a) $a_r = 0.2m/s^2$

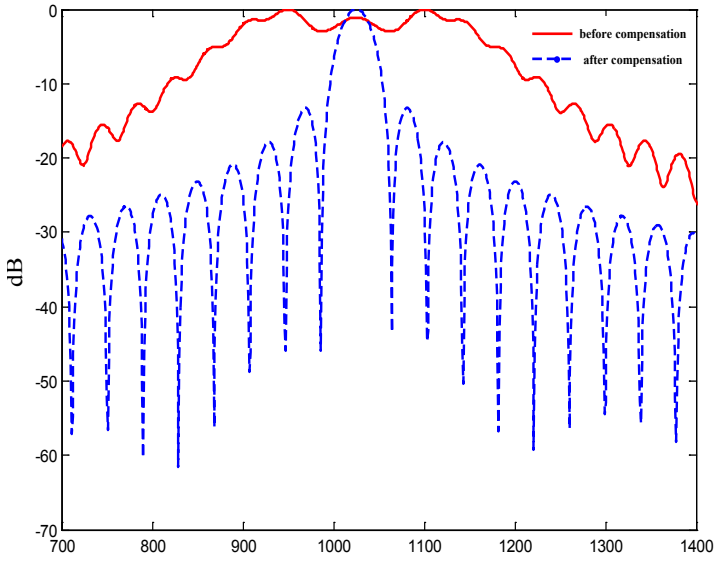

(b) $a_r = 0.3m/s^2$

Figure 3: Azimuth smearing degree for different range acceleration

Table 3: Performance analysis of point target after compensation

Quantitative norms		Time-domain method	Proposed method
IRW (m)	$0.2\,m/s^2$	0.999	1.029
	$0.3\,m/s^2$	0.998	1.043
PSLR (dB)	$0.2\,m/s^2$	-13.27	-13.26
	$0.3\,m/s^2$	-13.25	-13.28
ISLR (dB)	$0.2\,m/s^2$	-10.11	-10.15
	$0.3\,m/s^2$	-10.13	-10.17

It can be concluded that two-dimensional signal spectrum of moving targets with constant acceleration derived in this paper is accurate and the raw signal simulator presented in the paper is efficient.

5 Computational complexity analyses

To reveal the efficiency of the presented frequency-domain SAR scene simulator included moving targets with constant acceleration, the computational complexity of the proposed method is compared with the time-domain approach using the complex multiplication.

And the computation of the proposed simulator with a single type of target is

$$N_f = 6N_aN_r\log_2(N_aN_r) + 6N_aN_r \tag{13}$$

where N_a , N_r are the size of simulated scenes in the azimuth and range direction respectively. The computation of the time domain simulator is

$$N_t = N_a{}^2N_r^2 \tag{14}$$

However, it is tough to assess its efficiency directly because of the employed mixed targets in the proposed simulation. Suppose in a generated scene, there are m% targets belonging to moving point target (MPT) and n% is moving distributed target (MDT) with TUS of K , and the remaining are fixed point target (FPT)and fixed distributed target (FDT), then the accelerate ratio of the proposed method can be expressed as

$$\eta = \frac{(m\% * N_aN_r + n\% * N_aN_r / K + 1)N_f}{N_t} \tag{15}$$

Thus, the efficiency of the presented generator is mainly decided by the percentage of moving point and distributed targets. However, these targets usually occupy very small portion of the whole generated scene. Therefore, the mixed scene generator is still highly efficient. For example, a simulated scene with 8192 bins in the range direction and in the azimuth direction respectively, in which 0.001% belongs to MPT and 0.02% is MDT with TUS of 30*30 , then the accelerate ratio of this method is about 1873, which greatly increase the efficiency.

6 Conclusion

In the paper an efficient and precise strip-mode SAR raw data simulation approach for moving targets with constant acceleration is proposed. The simulator is based on the

accurate two-dimensional spectrum which can be derived accurately based on reversion of series. Numerical results demonstrate that the present method can reduce the computational time significantly without accuracy loss. The research of this paper is based on the situation of radar platform moving at constant speed, and in the following research, we will study the non-uniform motion of the radar platform.

Funding Statement: The work was supported by the Natural Science Foundation of Shandong Province, China. (Grant No. ZR2017BF032)

Conflicts of Interest: The authors declare that they have no conflicts of interest to report regarding the present study.

References

Chen, Y. X.; Guo, K. Y.; Wu, B. Y.; Sheng, X. Q. (2019): Multi-polarised SAR imaging simulation of ship on heavy sea. *The Journal of Engineering*, vol. 2019, no. 20, pp. 7006-7008.

Dogan, O.; Kartal, M. (2011): Efficient strip-mode SAR raw-data simulation of fixed and moving targets. *IEEE Geoscience and Remote Sensing Letters*, vol. 8, no. 5, pp. 884-888.

Franceschetti, G.; Iodice, A.; Perna, S.; Riccio, D. (2006): SAR sensor trajectory deviations: fourier domain formulation and extended scene simulation of raw signal. *IEEE Transactions on Geoscience and Remote Sensing*, vol. 44, no. 9, pp. 2323-2334.

Franceschetti, G.; Guida, R.; Iodice, A; Riccio, D.; Ruello, G. (2004): Efficient simulation of hybrid stripmap/spotlight SAR raw signals from extended scenes. *IEEE Transactions on Geoscience and Remote Sensing*, vol. 42, no. 11, pp. 2385-2396.

Franceschetti, G.; Migliaccio, M.; Riccio, D.; Schirinzi, G. (1992): SARAS: a synthetic aperture radar (SAR) raw signal simulator. *IEEE Transactions on Geoscience and Remote Sensing*, vol. 30, no. 1, pp. 110-123.

Jin, J. D.; Liu, K. Y.; Deng, Y. K; Sha, Y.; Wang, R. et al. (2019): Nonlinear frequency modulation signal generator in LT-1. *IEEE Geoscience and Remote Sensing Letters*, vol. 16, no. 10, pp. 1570-1574.

Li, Y. K.; Liu, B. C.; Wang, L.; Chen, H. M.; Nie, L. S. et al. (2019): An accurate imaging and doppler chirp rate estimation algorithm for airborne CSSAR-GMTI systems. *IEEE Access*, vol. 7, pp. 170077-170086.

Lv, G. H.; Wang, J. F.; Liu, X. Z. (2013): Ground moving target indication in SAR images by symmetric defocusing. *IEEE Geoscience and Remote Sensing Letters*, vol. 10, no. 2, pp. 241-245.

Mori, A.; Vita, F. D. (2004): A time-domain raw signal simulator for interferometric SAR. *IEEE Transactions on Geosciences and Remote Sensing*, vol. 42, no. 9, pp. 1811-1817.

Qiu, X.; Hu, D.; Zhou, L.; Ding, C. B. (2010): A bistatic SAR raw data simulator based on inverse ω-k algorithm. *IEEE Transactions on Geoscience and Remote Sensing*, vol. 48, no. 3, pp. 1540-1547.

Sjogren, T. K.; Vu, V. T.; Peterson, M. I.; Gustafsson, A; Uplander, L. M. H. (2012): Moving target relative speed estimation and refocusing in synthetic aperture radar

images. *IEEE Transactions on Aerospace and Electronic Systems*, vol. 48, no. 3, pp. 2426-2436.

Wang, Y.; Zhang, Z. M.; Deng, Y. K. (2008): Squint spotlight SAR raw signal simulation in the frequency domain using optical principles. *IEEE Transactions on Geoscience and Remote Sensing*, vol. 46, no. 8, pp. 2208-2215.

Wang, X. L.; Zeng, P. J.; Patterson, N.; Jiang, F.; Doss, R. (2019): An improved authentication scheme for internet of vehicles based on blockchain technology. *IEEE Access*, vol. 7, pp. 45061-45072.

Xiong, X.; Jin, G. W.; Xu, Q.; Zhang, H. M.; Xu, J. (2019): Robust line detection of synthetic aperture radar images based on vector radon transformation. *IEEE Journal of Selected Topics in Applied Earth Observations and Remote Sensing*, vol. 12, no. 12, pp. 5310-5320.

Yang, L.; Yu, W. D.; Gao, Y.; Zhang, L. (2013): Efficient strip-mode SAR raw signal simulation of mixed targets based on accurate 2-D spectrum. *Journal of Electronics*, vol. 31, no. 1, pp. 8-15.

Yang, L.; Yu, W. D.; Luo, Y. H.; Zheng, S. C. (2013): Efficient strip-mode SAR raw data simulator of extended scenes included moving targets. *Progress in Electromagnetics Research B*, vol. 2013, no. 53, pp. 187-203.

Zhang, X. R.; Duan, J. L.; Liu, J.; Badler, N. I. (2019): An integrated suture simulation system with deformation constraint under a suture control strategy. *Computers*, *Materials & Continua*, vol. 60, no. 3, pp. 1055-1071.